Supporting Information for "Imaging seismic and aseismic plate coupling with interferometric radar (InSAR) in the Hikurangi subduction zone"

L. Maubant[1], W. B. Frank[1], L.M Wallace[2,3,4],C. Williams[5], Ian Hamling[5]

[1]Department of Earth, Atmospheric and Planetary Sciences, Massachusetts Institute of Technology, Cambridge, MA, USA

[2]University of Texas Institute for Geophysics, Austin Texas

[3]GEOMAR Helmholtz Centre for Ocean Research Kiel, Kiel, Germany

[4]Institute of Geosciences, Christian-Albrechts-Universität zu Kiel, Kiel, Germany

[5]GNS Science, Lower Hutt, New Zealand

Contents of this file

Text S1. Definition of the dataset weighting coefficient

The relative weight between the two datasets is introduced by a weighting factor of the data covariance matrix, C_d:

$$C_d = \begin{bmatrix} \alpha^2 C_{dInSAR} & 0 \\ 0 & (1-\alpha)^2 C_{dGNSS} \end{bmatrix} \quad (1)$$

where C_{dGNSS} is the covariance of the GNSS data, C_{dInSAR} is the covariance of the InSAR data and α is the weighting coefficient. If $\alpha = 0$ the weight of the InSAR data is null, if α=1 the weight of the GNSS data is null.

Text S2. Choice of weighting coefficient

We evaluate a range of values of α, the weighting coefficient between the GNSS and InSAR datasets, between 0.2 and 0.9. We observe that the goodness-of-fit χ^2 value of each dataset is less than 0.4 and does not change significantly with α. This suggests that this range of α values is a reasonable, with both datasets fitting well the predictions. Models with different weights within this broad range are all quite similar to one another. However, if the weight exceeds α=0.6, we are not able to resolve the plate coupling in the North of the subduction, because we do not have InSAR data in this region. We chose a value of 0.4 because it is a reasonable balance between the two datasets and produces a model with a low χ^2 value.

Text S3. Inversion method

We used a static inversion method to estimate the slip deficit rates on the subduction interface based on the observed displacement rates on the surface (Savage, 1983). The map of predicted velocities on the plate interface recovered using this inversion represents the estimated slip deficit rate. To obtain the coupling coefficient we need to divide each

patch result by the loading velocity:

$$\gamma = \frac{V_{backslip}}{V_0}. \tag{2}$$

We use the model of Wallace and Beavan (2010) to estimate V_0 (Figure S6). Plate coupling (γ), where the subducting plate is assumed to be frictionally locked to the upper plate, is typically <1, with 1 designating a fully locked interface. A negative or null value of coupling corresponds to slip on the interface during the observational period; values of slip are typically higher than V_0, producing coupling values < -1.

In our forward model, the Green's functions are computed for a homogeneous elastic half-space using the analytical formulation of Okada (1992). To alleviate the inversion's computational cost, we reduce the number of InSAR velocity measurements in each track by performing a uniform downsampling pixel values with a 10 $\times$ 10 km^2 window. The associated InSAR uncertainties are computed from the errors associated with each pixel (Figure S5) using the same downsampling method. We neglect the covariance between pixels, and covariance terms between our GNSS and InSAR datasets in this inversion to reduce the computational cost. We note that considering the covariance between pixels and the covariance terms between our GNSS and InSAR datasets in the inversion would lead to excessive downweighting of the InSAR data, likely undervaluing InSAR's contribution to the overall analysis (Bekaert et al., 2016). The slip direction is fixed in the inversion using the rake of the block model that defines our upper plate reference frame (Wallace & Beavan, 2010), where the rake of each fault patch is the projection of the plate velocity vectors from the block model (Figure S6). Finally to calculate our model m, we perform a linear inversion:

$$m^* = m_0 + C_m G^t (G C_m G^t + C_d)^{-1} (d - G m_0) \tag{3}$$

where m_0 is the model *a priori* (Tarantola, 2005), and C_d and C_m are respectively the covariance matrices of the data and the model.

The purpose of utilizing the model covariance matrix C_m is to incorporate correlation between adjacent parameters, which is known as spatial smoothing. The value at position (i, j) in C_m is determined by the following equation:

$$C_m(i,j) = (\sigma_{m0}\frac{\lambda_0}{\lambda})^2 exp(-\frac{d(i,j)}{\lambda}) \tag{4}$$

We explore the optimal values of σ_{m0} and λ for each time periods. For the 2- and 4-years, we first explore the optimal value of $\log_{10}(\sigma_{m0}) = -2.6$ for a fixed λ=50 km. Once the optimal value is found (Figure S13) we then search for the optimal λ value which we fix to λ=30 km. The optimal model has a $\chi^2 = 0.21$ (2-year) and $\chi^2 = 0.25$ (4-year). For the 10-year observational period where we only use GNSS data, we search for different optimal values (Figure S11, $\log_{10}(\sigma_{m0}) = -1$ and $\lambda = 30$km).

References

Bekaert, D. P., Segall, P., Wright, T. J., & Hooper, A. J. (2016). A Network Inversion Filter combining GNSS and InSAR for tectonic slip modeling. *Journal of Geophysical Research: Solid Earth*, *121*(3), 2069–2086. doi: 10.1002/2015JB012638

Okada. (1992). Internal deformation due to shear and tensile faults in a half space. *Bulletin of the Seismological Society of America*, *82*(2), 1018–1040. Retrieved from `http://bssa.geoscienceworld.org/content/82/2/1018.short`

Savage, J. C. (1983). A dislocation model of strain accumulation and release at a subduction zone. *Journal of Geophysical Research*, *88*(B6), 4984–4996. doi: 10.1029/JB088iB06p04984

Tarantola, A. (2005). *Inverse problem theory and methods for model parameter estimation*. Society for Industrial and Applied Mathematics.

Wallace, L., & Beavan, J. (2010). Diverse slow slip behavior at the hikurangi subduction margin, new zealand. *Journal of Geophysical Research: Solid Earth*, *115*(B12).

Table S1. Table of the number of images and interferograms for two Sentinel-1 tracks used in this study.

Track Name	Number of Images	Number of Interferograms
A081	183	1376
D175	154	1281

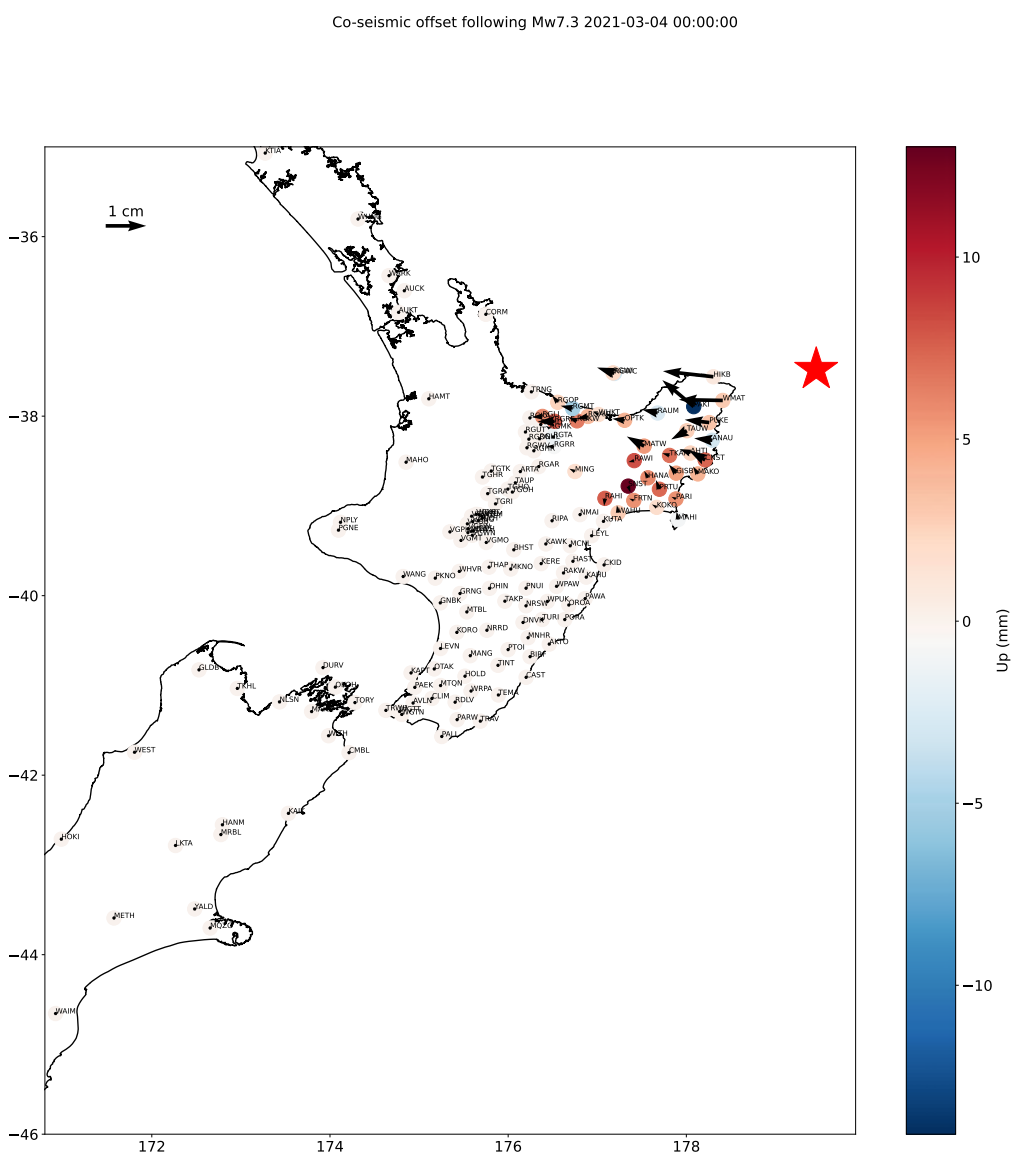

Figure S1. Coseismic offset corrected from GNSS stations for the seismic sequence of March, 4th, 2021.

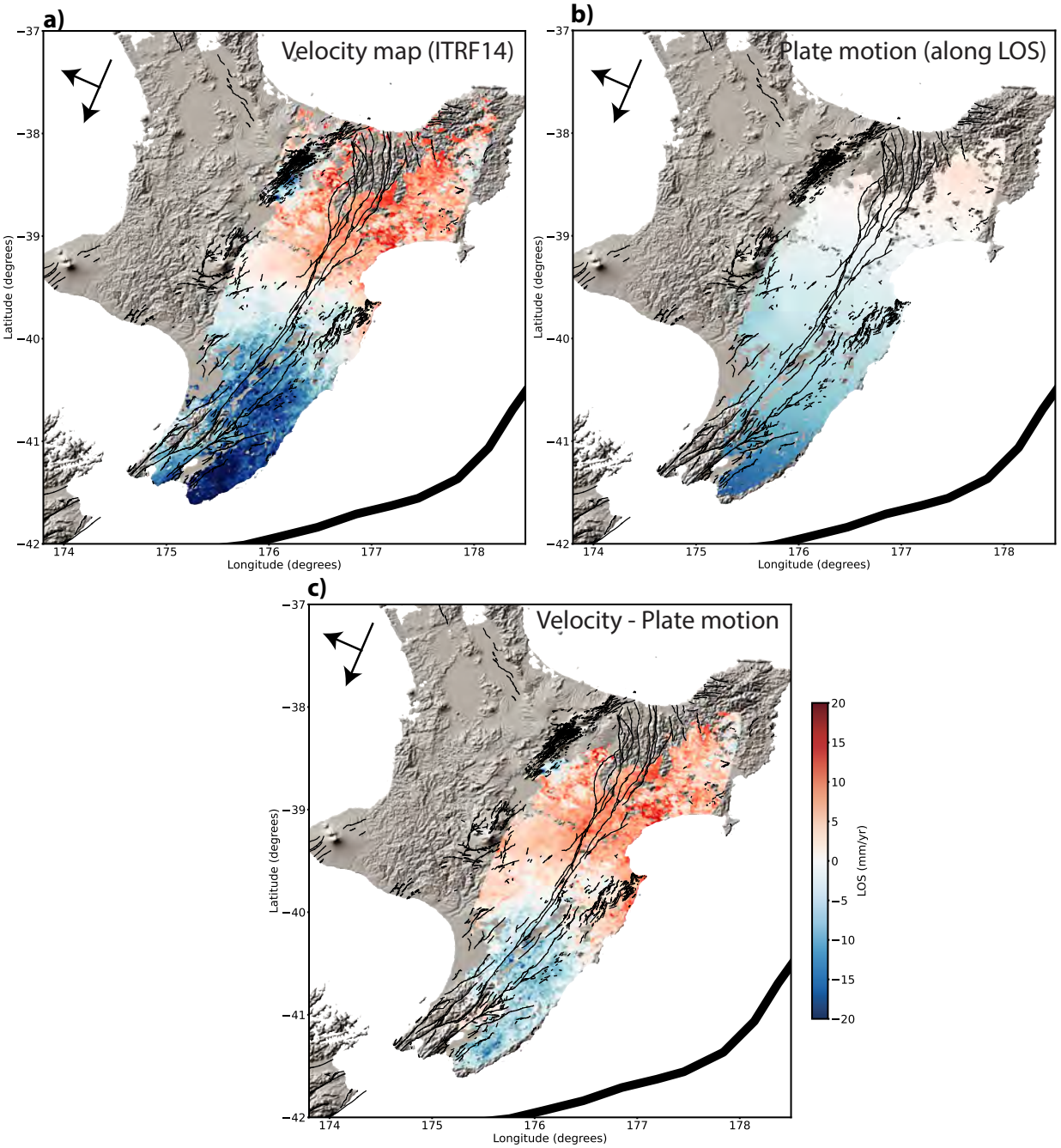

Figure S2. D175 velocity maps. a) Velocity map in ITRF14 reference frame, b) Plate motion in Line-Of-Sight of the satellite. c) Velocity map corrected from the plate motion

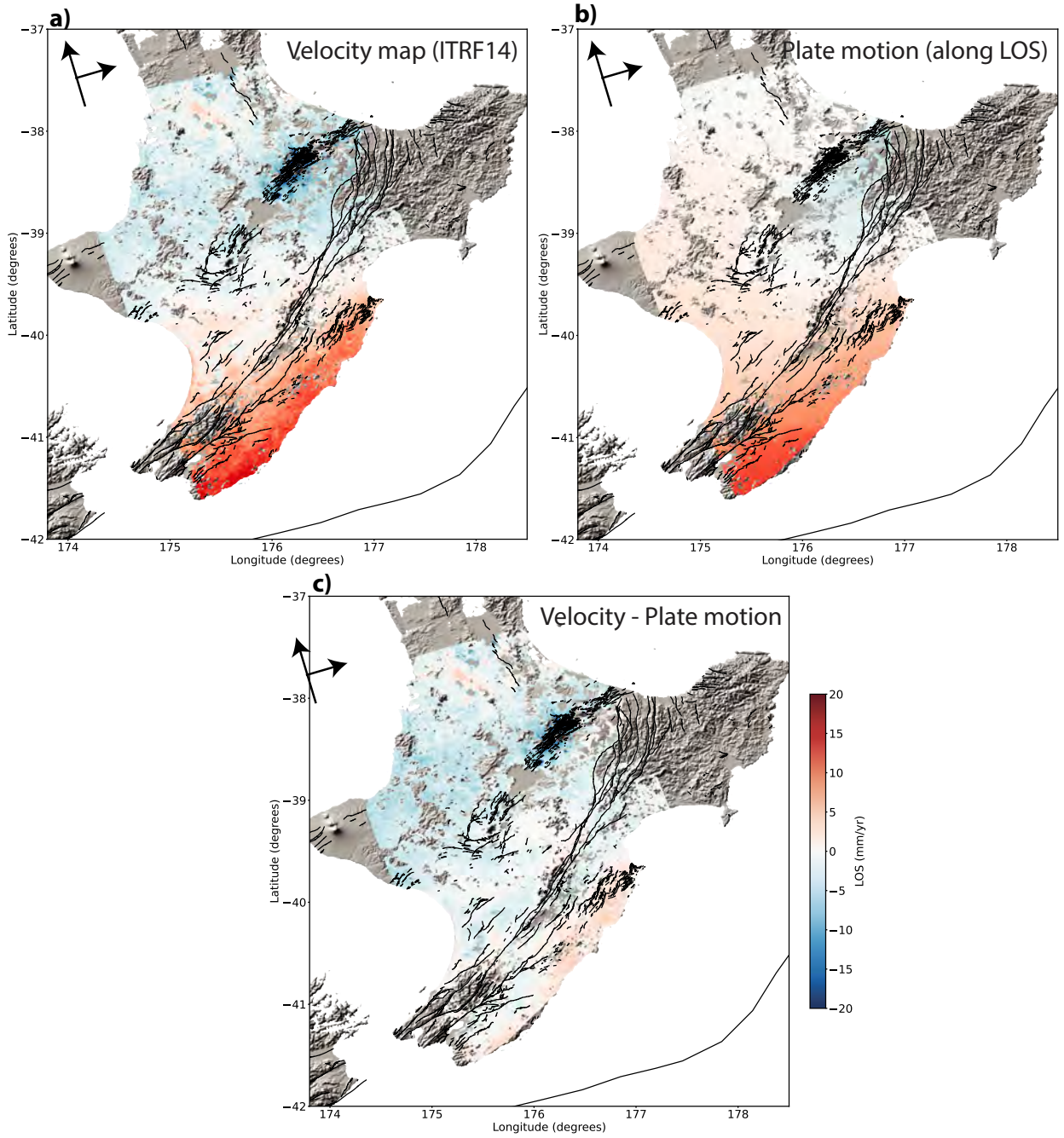

Figure S3. A081 velocity maps. a) Velocity map in ITRF14 reference frame, b) Plate motion in Line-Of-Sight of the satellite. c) Velocity map corrected from the plate motion

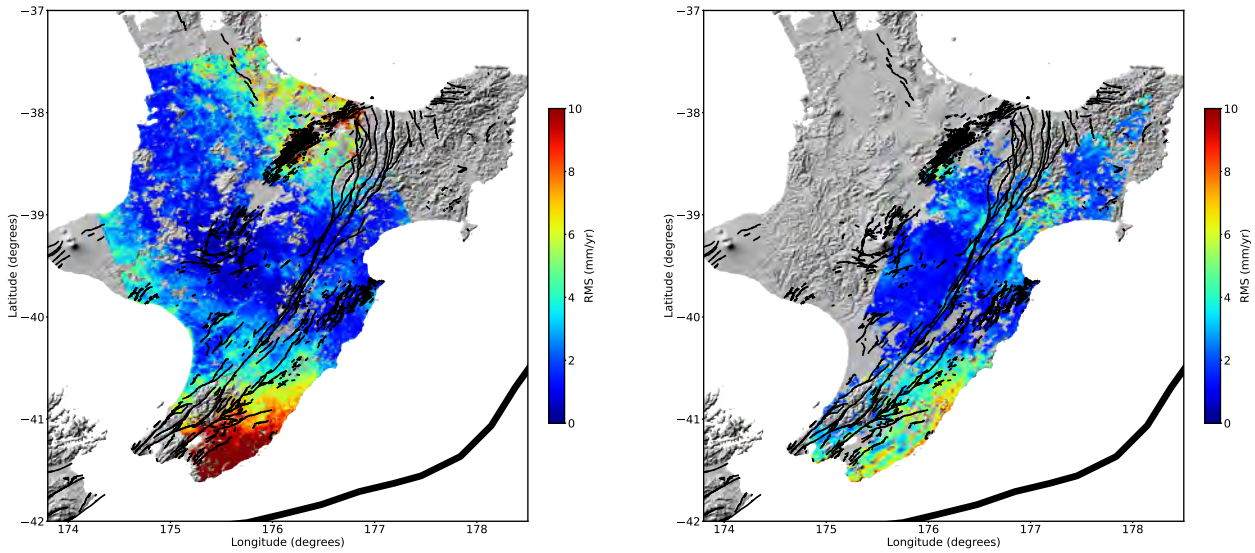

Figure S4. Errors associated to each pixel for InSAR velocity maps. Left: RMSE of A081 track. Right: RMSE of D175 track.

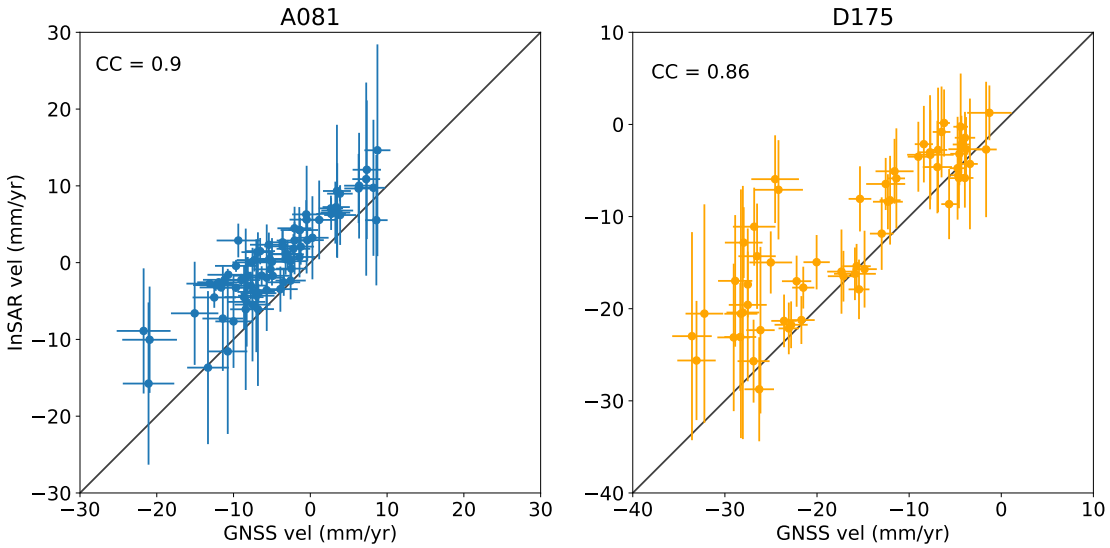

Figure S5. Comparison between InSAR and GNSS velocities (converted in LOS). Left: comparison for the ascending track. Right: comparison for the D175 track.

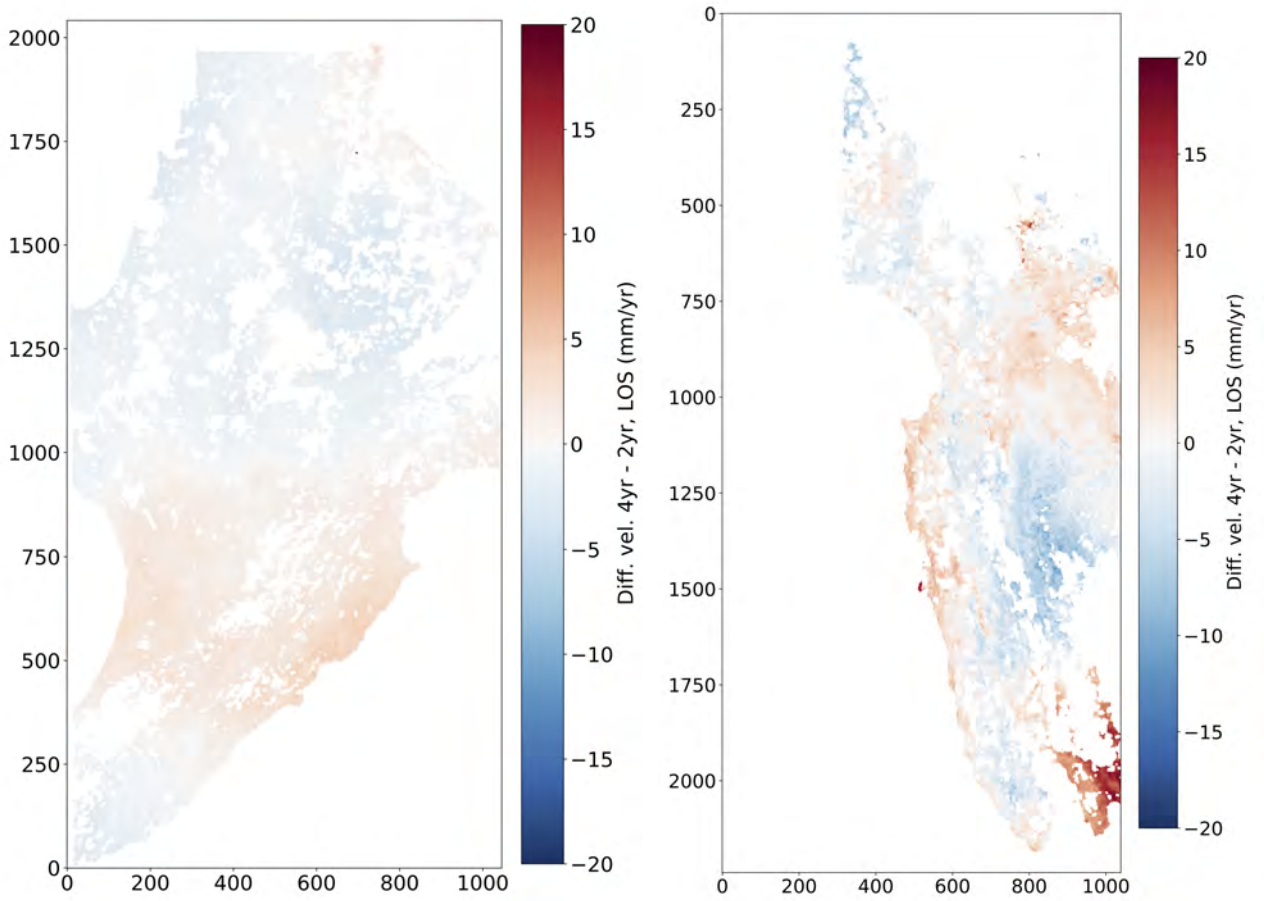

Figure S6. Difference between InSAR velocities maps calculated on a period of 4 years and a period of 2 years. Left: ascending track, right: descending track.

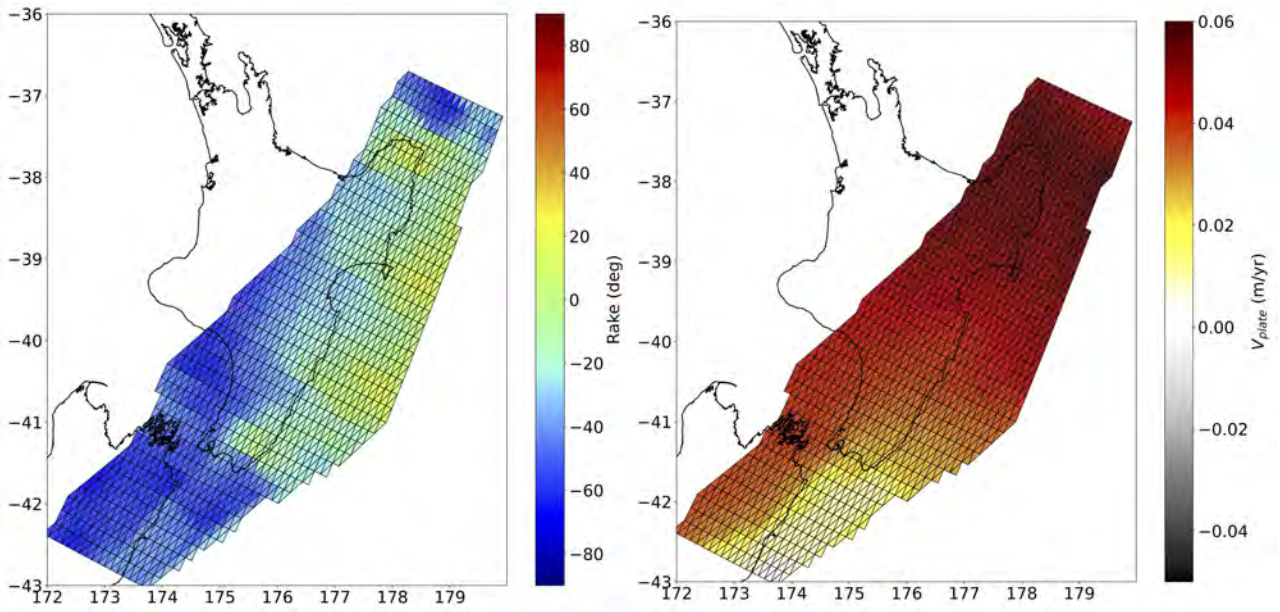

Figure S7. Rake (left) and velocity plate (right) model of the Hikurangi subduction zone from (Wallace & Beavan, 2010).

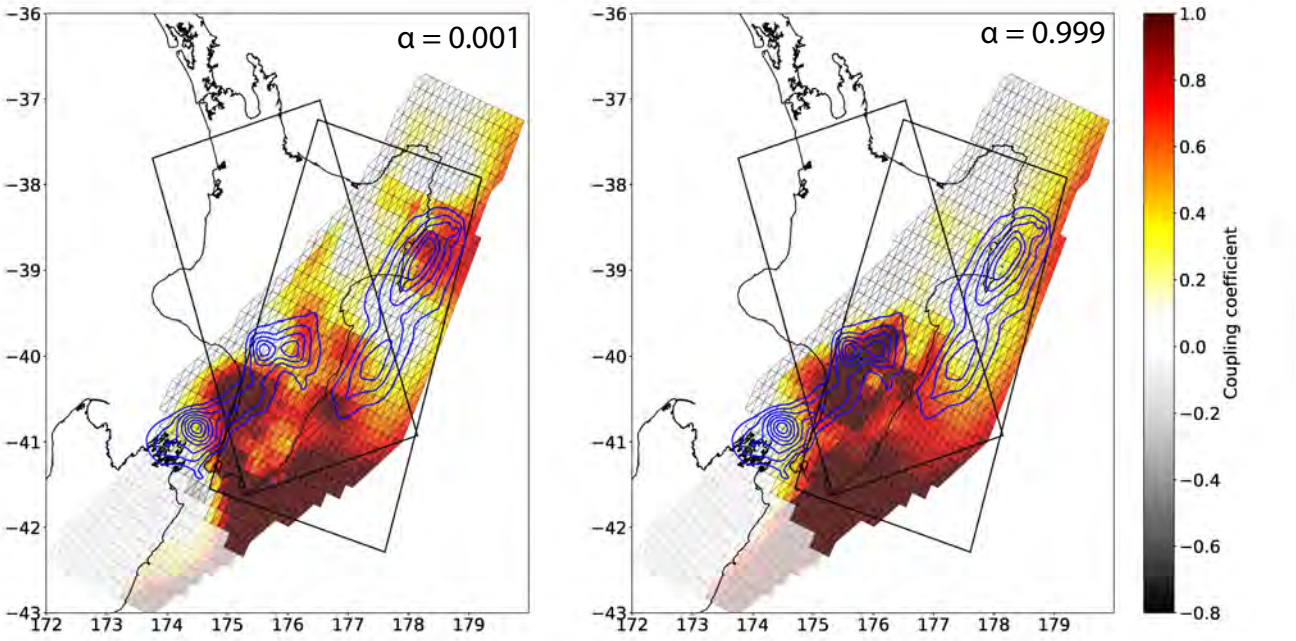

Figure S8. Model of coupling between deep slow slip events (2-years) using only GNSS data on the left ($\alpha = 0.001$) or only InSAR data on the right ($\alpha = 0.999$). The blue lines represent the slow slip events. The black rectangles are the footprint of the InSAR tracks.

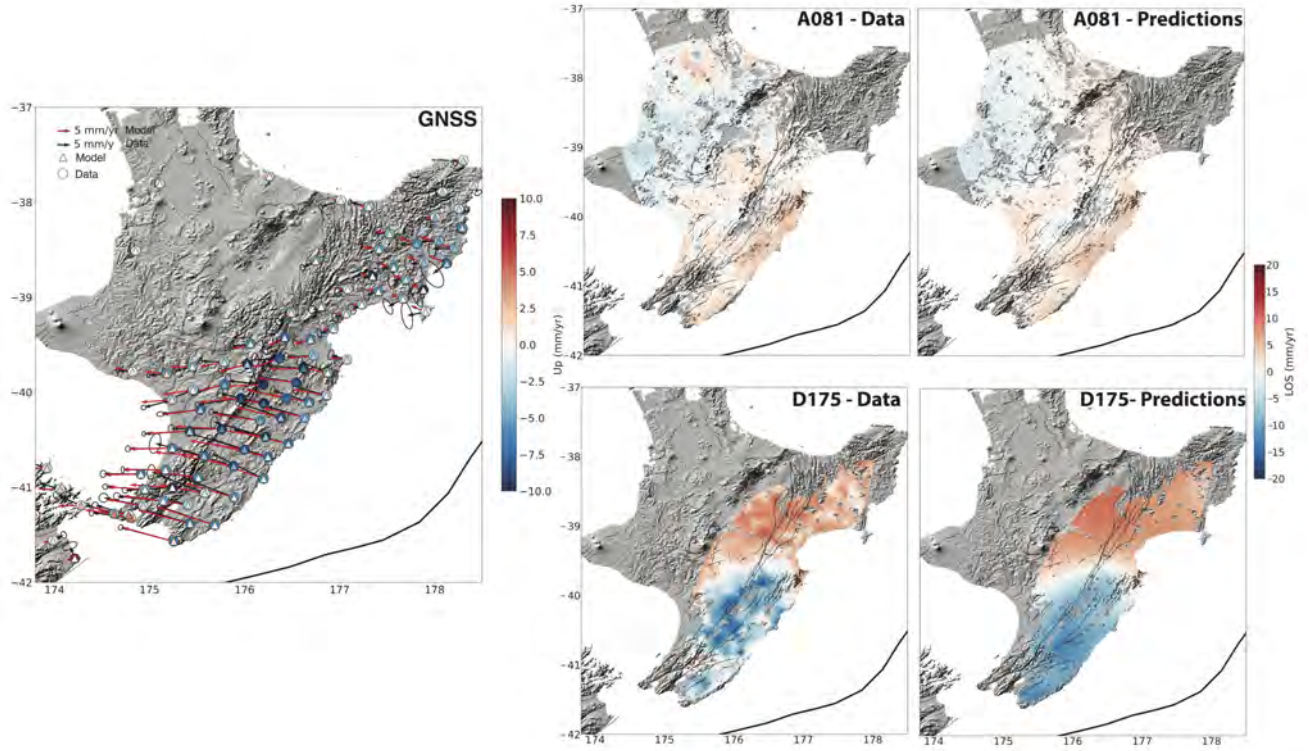

Figure S9. Comparison between data and predictions of the model for the inversions of 2-years of observational period. The Left panel is the GNSS data (black arrows and circles) and prediction (red arrows and triangles). The right panels are data and predictions for InSAR data (A081 on up line, D175 on bottom line).

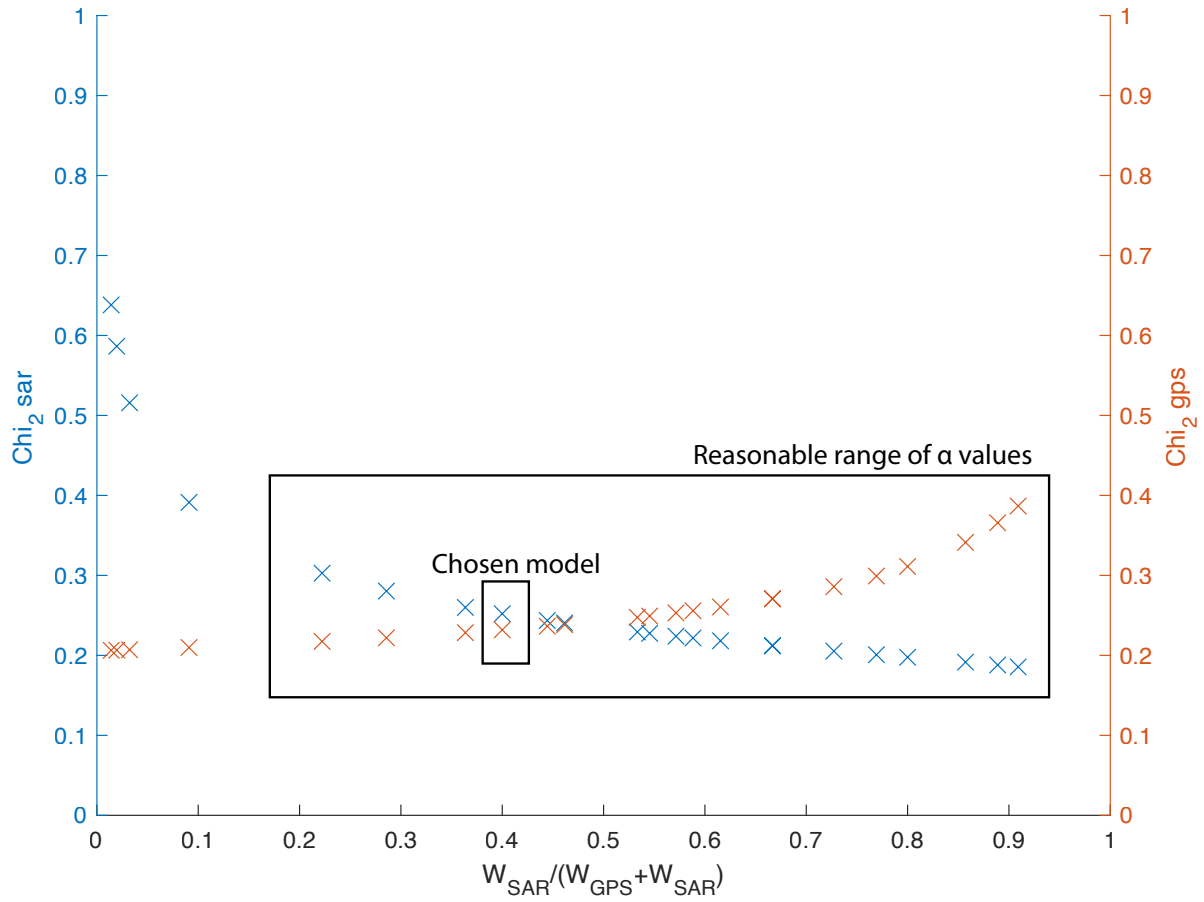

Figure S10. χ^2 values for InSAR (in blue) and GNSS (in orange) as function of the weight (α). The chosen model is framed in black (small rectangle).

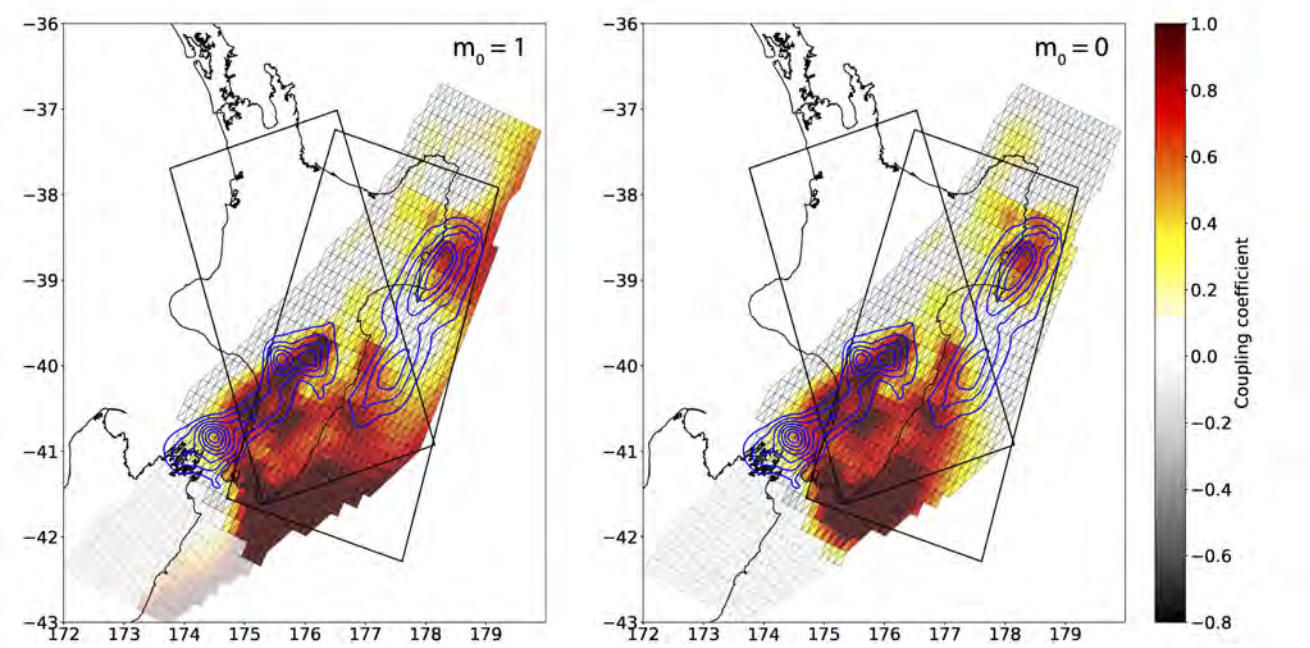

Figure S11. Model of coupling between deep slow slip events (2-years) using a model a priori coupled (left) or uncoupled (right). The blue lines represent the slow slip events. The black rectangles are the footprint of the InSAR tracks.

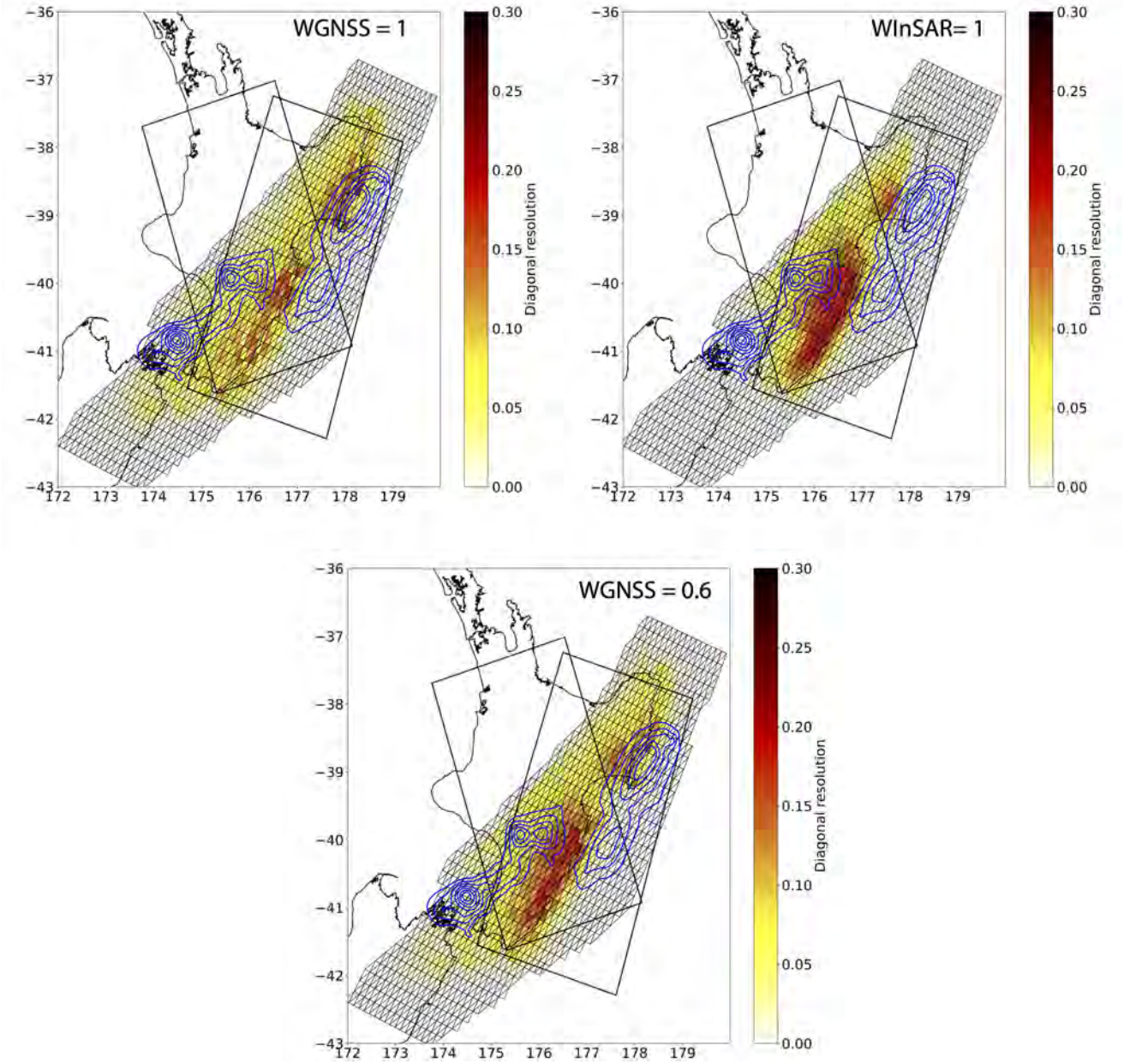

Figure S12. Diagonal of the matrix of resolution for: (right) a model with an α 0.001 (GNSS only); (left) a model with an α 0.999 (InSAR only) and (bottom) our chosen model (α=0.4). The model a priori m_0 is coupled.

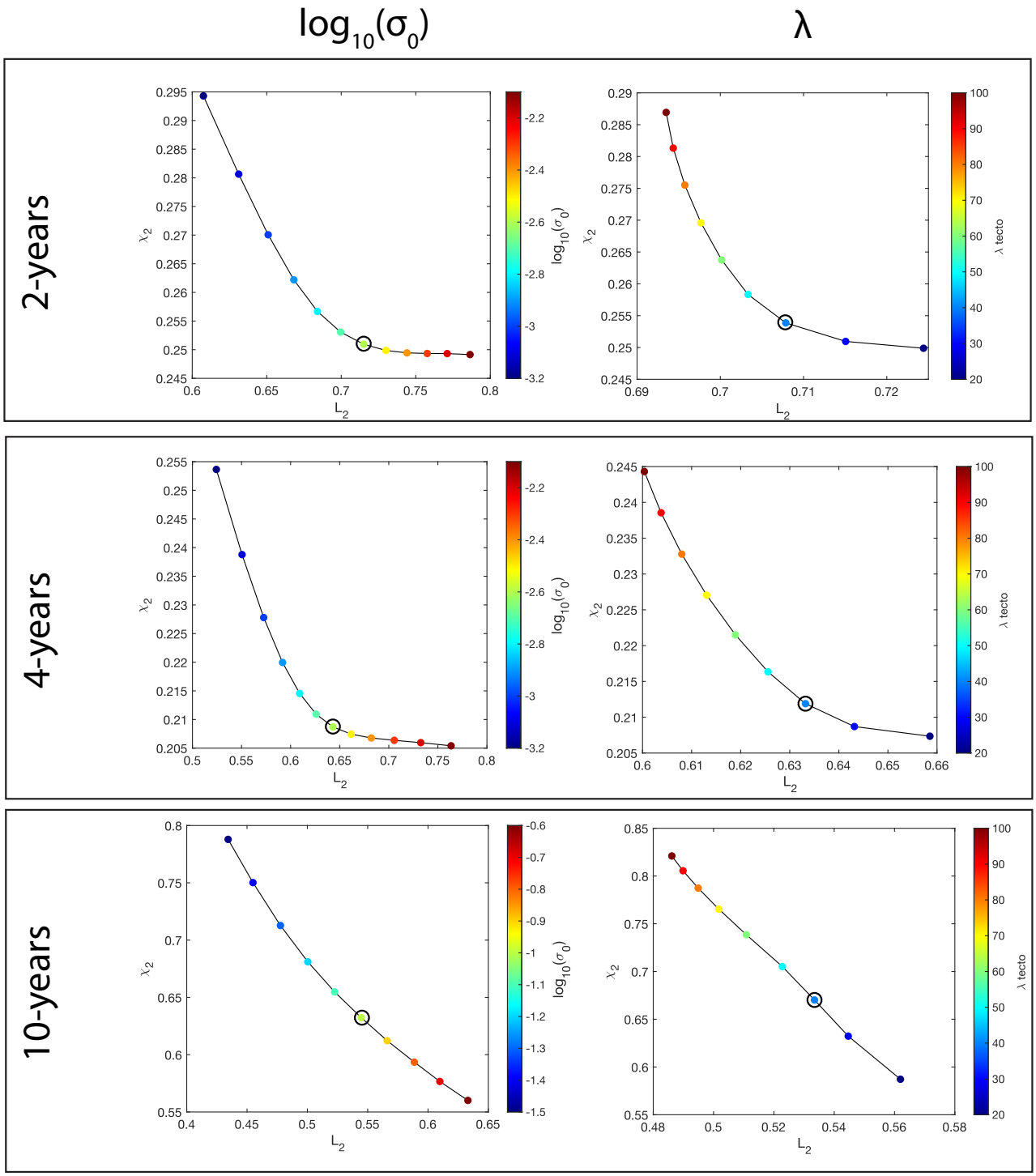

Figure S13. Parameters value optimization, data misfit (Chi-square χ^2) in function of the regularized solution (L2 norm) for different dampling values (left) and λ values (in km). On the left column is the dampling value σ_{m0} for a $\lambda = 50$km for the different period of observation. On the right column is the along strike correlation lenght (λ) for a $\sigma_{m0} = 10^{-2.6}$. The selected optimal model is circled in black.

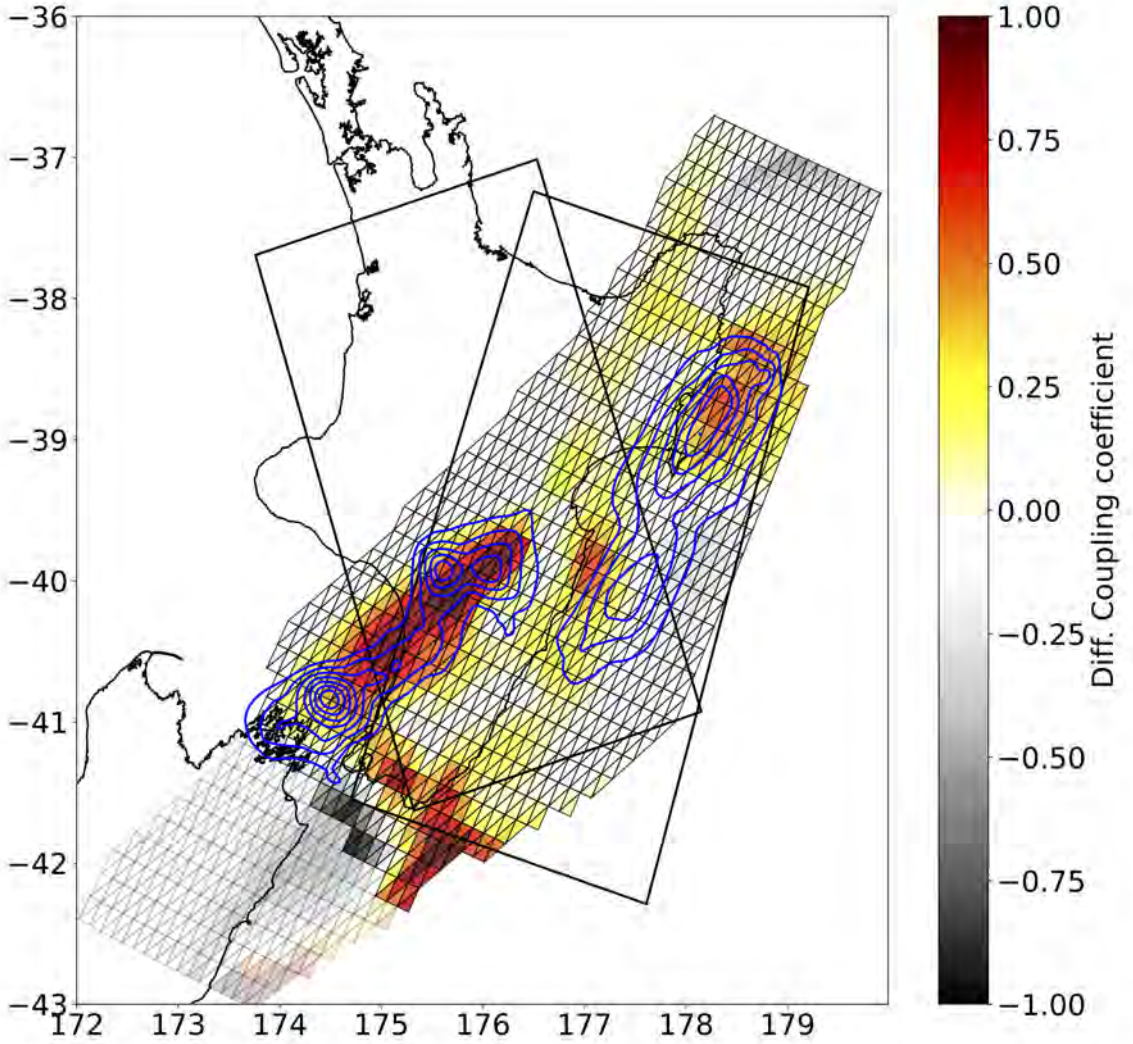

Figure S14. Difference of coupling coefficient between a coupling map over 2-years and 10-years. a positive value represent a region where the stress have been more accumulated during the short period than during the long period.